

4.9 OPTICAL AUTOCOVARIANCE WIND LIDAR (OAWL): A NEW APPROACH TO DIRECT-DETECTION DOPPLER WIND PROFILING

Christian J. Grund, and Sara C. Tucker*
Ball Aerospace & Technologies Corp., Boulder, Colorado

1. INTRODUCTION

Winds are key dynamic equilibrators of the atmospheric mass and energy fields. Insufficiencies and inaccuracies in current wind observations, particularly over the oceans, in the southern hemisphere, and in the tropics, lead to uncertainty in the modeling of global atmospheric circulations, limiting weather forecasting skill and diminishing our understanding of water, chemical species, and energy transport. Doppler wind lidar (DWL) is becoming more common in airborne and ground-based atmospheric process investigations and the NASA Decadal Survey defines a 3-D Winds mission that identifies Doppler Wind Lidar (DWL) in low earth orbit (LEO) as the key technology needed to meet the global wind profiling objectives [1]. To profile winds, DWL's measure the line of sight optical Doppler frequency shift from aerosols and molecules as a function of range. Backscatter from molecules is ever-present but spectrally broadened by thermal motions limiting the achievable wind measurement precision for a given signal-to-noise ratio (SNR). Aerosols are characterized by Brownian motions that produce far less backscatter spectral broadening providing the best wind information, but are not always present. A hybrid lidar [2] measuring winds from both aerosol and molecular backscatter therefore maximizes the availability of wind profiles. The Optical Autocovariance Wind Lidar (OAWL) [3] is a direct detection DWL approach that uses a unique high resolution (10^9 - 10^{10}) interferometer to measure line-of-sight (LOS) aerosol backscatter winds to <0.5 m/s precision. When operated at UV wavelengths (~ 355 nm), OAWL can simultaneously measure molecular and aerosol backscatter winds. However, detailed instrument modeling suggests that a more photon-efficient Integrated Direct Detection (IDD) architecture, shown in Figure 1, that combines a dual-edge etalon pre-filter/discriminator with a high resolution OAWL receiver allows extremely efficient optimization simultaneous wind profiling of both molecular and aerosol backscatter-components. The IDD hybrid approach uses a single transmit laser and receiving system with relaxed several-wave telescope optical requirements, making it much simpler, lower mass, lower cost, and more power efficient than an alternative hybrid approach that uses a combination of a 2- μ m wavelength Coherent Detection DWL [4] for aerosol wind profiling combined with a separate 355nm dual-edge etalon direct detection DWL [5] for measuring the molecular component.

In addition to winds, the OAWL technique can be used to measure calibrated aerosol optical properties at multiple simultaneous wavelengths using the High spectral

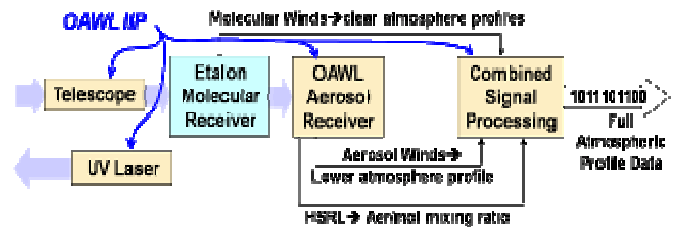


Figure 1 Architecture of the Integrated Direct Detection (IDD) hybrid that promises to provide full wind profiles using a conventional double-edge etalon to resolve the molecular backscatter component and an OAWL receiver to resolve the aerosol backscatter component (normally rejected by the etalon front end). Only one laser transmitter is required and the required optical wave front quality is significantly reduced compared to a coherent detection system.

resolution lidar method (HSRL) [3]. This facilitates combined single-instrument wind and HSRL lidar missions, providing additional potential cost savings and improved science data for Decadal Survey missions.

The primary objectives of the IIP are to raise the OAWL DWL technology from TRL3 to TRL5 by taking the multi-wavelength field-widened OAWL receiver built under Ball internal funds, engineering it into complete lidar system configured to fit into a WB-57 aircraft palate by integrating it with a telescope, laser, data system, environmental control, and framework, ground validate the system against a coherent Doppler lidar, and then flying the system at high altitude in a WB-57 aircraft to validate performance against wind profilers and a ground-based coherent DWL system. We are in the last year of a 3-year IIP, and have demonstrated first aerosol wind measurements for an OAWL system. This paper presents preliminary first wind measurements and discusses ground and airborne validation plans.

2. OPTICAL AUTOCOVARIANCE LIDAR THEORY

Figure 2 (top) shows the main spectral features of the lidar atmospheric return from a monochromatic laser pulse. The signal is the linear sum of the backscatter from aerosols and molecules (equation 1).

$$S_{a+m} = S_a + S_m + B \quad (1)$$

* Christian J. Grund, Ball Aerospace & Technologies Corp., 1600 Commerce St., Boulder, CO 80301; cgrund@ball.com

S_m is the thermally Doppler-broadened backscatter component from molecules, S_a is the aerosol backscatter component with nearly the same spectral distribution as the transmitted light, and B is the uncorrelated background light contribution. The mean frequency of the aerosol and molecular components due to a line-of-sight (LOS) wind follows the Doppler shift.

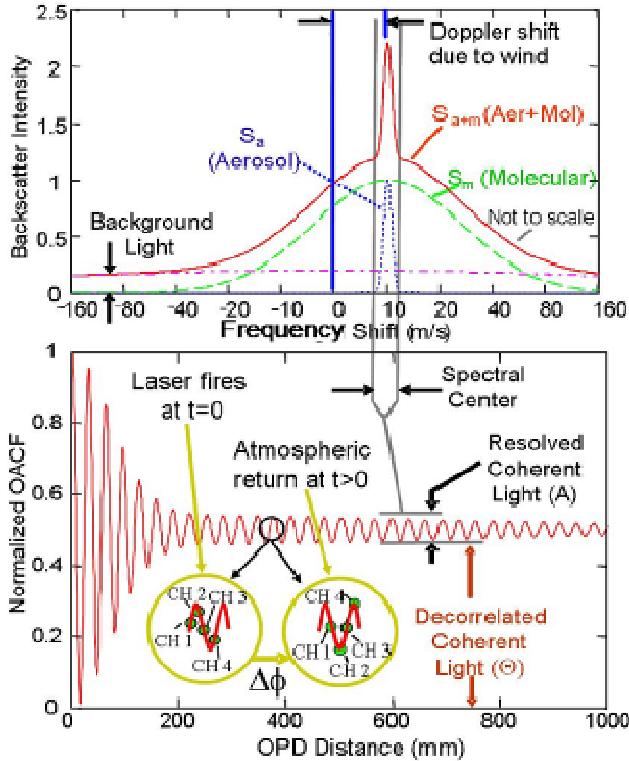


Figure 2 (Top) The backscatter spectral distribution from a monochromatic transmitted laser pulse at 0 wavelength shift is a linear sum of the near-monochromatic aerosol backscatter and the Doppler-broadened molecular backscatter. The center frequency is Doppler shifted by line of sight winds. (Bottom) The amplitude of the OACF of the backscatter spectrum depends on the spectral width and the OPD. The frequency of the OACF is determined by the received optical signal frequency. The phase shift of the OACF is proportional to the number of OACF cycles in within the OPD * received optical frequency shift, enabling very high spectral (speed) resolution. The OACF does NOT depend on the optical phase of the backscatter, only on its frequency.

Figure 2 (bottom), shows the Optical Autocovariance Function (OACF) expected from a typical return as a function of Optical Path Difference (OPD) in an interferometer (e.g. a Michelson or Mach-Zehnder). At any particular interferometer OPD, the line of sight (LOS) velocity, V , due to wind is calculated from equation 2,

$$V = \lambda * \Delta\phi * c / (2 * (OPD)), \quad (2)$$

where $\Delta\phi$ is the OACF phase shift (expressed as a fraction of an OACF cycle), c is the speed of light, and λ is the wavelength. In the OAWL approach, no moving

mirrors are required to resolve the local phase of the OACF about a fixed OPD (~0.9m). Instead, measurements are made of the local OACF amplitude simultaneously at several OPD's sequentially differing by $\lambda/4$ (denoted CH1-CH4, each intensity is measured by a different detector). $\Delta\phi$ is determined by fitting a sine function to the OACF of a sample of the transmitted pulse and calculating the OACF phase difference to the sine fit of the received light.

To accommodate laser frequency and interferometer OPD drift, a small fraction of the outgoing laser pulse is reflected into the interferometer path so that the phase of the OACF is determined for 0-velocity at 0-range (T_0) on every shot. $\Delta\phi$ is then the difference between the OACF measured from each range and the T_0 OACF phase.

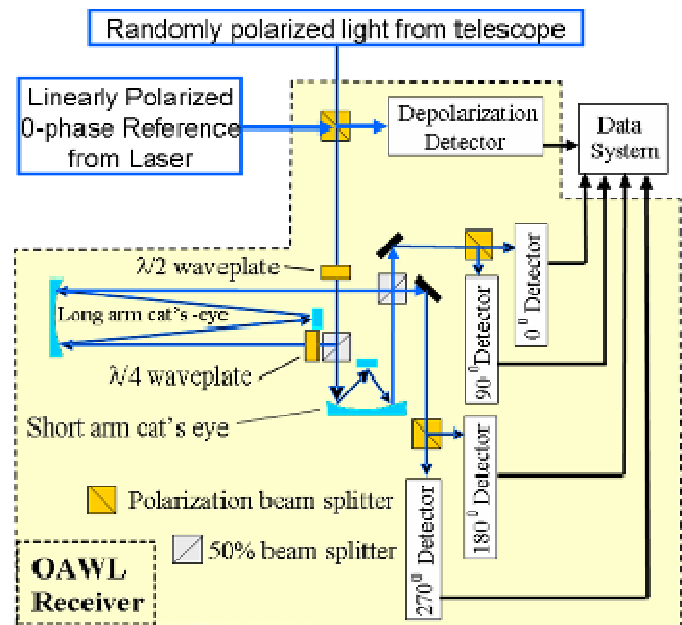


Figure 3 Architecture of the OAWL receiver. Field-widening using cat's-eye mirrors in the interferometer is key to multi- λ operation and maintaining practical system étendu with a 10^{10} spectral resolution.

Figure 3 shows the architecture of the OAWL receiver. Polarization multiplexing is used to simultaneously create four OPD delays in the same interferometer volume. The cat's-eye mirrors facilitate high spectral resolution, system étendu, and multi- λ . A dichroic mirror and a separate set of four detectors are used to separate the OPD channel signals for each wavelength, but the interferometer and receiver optics are otherwise common to all channels and wavelengths.

3. THE OAWL SYSTEM

At the last ESTO conference we discussed the theory, architecture, development progress, and demonstration plans for the OAWL DWL system. The integrated system is shown in Figure 4. The system is designed to fit in a 6'

WB-57 pressureized pallet with a fixed 45° pointing orthogonal to the flight direction. For ground operation, the optical assembly is mounted in a Flowtron stand to facilitate azimuth and elevation pointing.

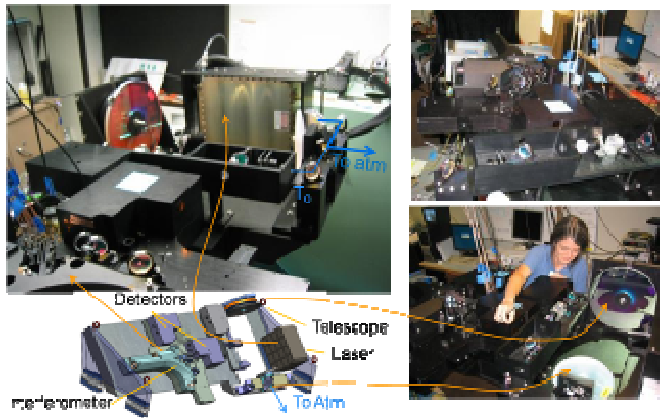


Figure 4 The integrated OAWL IIP system in the lab.

During the receiver design phase, we built a comprehensive integrated system model and calculated the performance of the interferometer when subjected to expected operational WB-57 vibration levels. The model results are compared to the design goals in Figure 5. The history of performance improvements with design iterations are shown by the bars (note log scale). Prior to integrating the receiver into the system assembly, we subjected it to vibration testing at expected operational (OP) and taxi-takeoff-and landing levels (TTOL) using measured spectra from the WB-57 pallet bay. The test results confirmed the construction methods and workmanship, and validated the model analysis to within expected dynamic model uncertainties. These results suggest that we understand the OAWL architecture and sensitivities well enough to construct a stable passive 10^{9-10} resolution interferometer, and to design and predict on-orbit performance of a fully developed OAWL system.

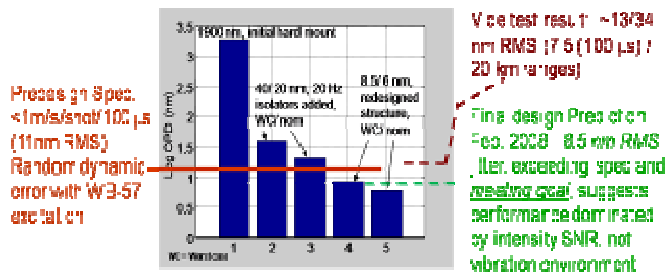


Figure 5 History of OAWL receiver design iterations and resultant performance improvements predicted by a comprehensive integrated system model in the presence of operational aircraft vibration levels. The original design goal and spec are shown along with the actual as built vibration test results. Agreement is well within expected uncertainties for dynamic models.

The test results also confirm that the wind measurement performance of the OAWL receiver as-built will be

dominated by SNR not platform vibration effects during the WB-57 flight tests.

4. FIRST OAWL GROUND MEASUREMENTS

After final delivery of the laser in November 2010, system integration was rapidly completed, and first engineering tests were performed in early January from a small lab on the rooftop of one of the buildings on the Ball Boulder campus. The observation configuration is shown in Figure 6. Due to eye-safety considerations and the proximity of a small airport to the Ball campus, the lidar was confined to fixed pointing operations on a $\sim 3.8^\circ$ upward slope along a mountain valley to the west of town. The Boulder Atmospheric Observatory (BAO) tower is located ~ 10 miles ENE of the lidar is flat rural terrain. The BAO tower is 1000' tall and has anemometers at 10m, 100m and 300m altitudes AGL.



Figure 6 The experiment domain is shown with bird's-eye views of the lidar location atop a spacecraft assembly building on the Ball campus and the BAO tower ~ 10 mi to the ENE of the lidar in relatively flat unobstructed terrain. Because of the proximity of the Ball location to a nearby airport, eye-safety restrictions constrain the lidar to point up at a $\sim 3.8^\circ$ slope along a mountain valley to the west. Not the most ideal conditions for intercomparison. Nonetheless, there is reasonable agreement between the lidar and tower wind profiles.

Preliminary results from these tests are shown in Figures 8-11. All OAWL data are from the analog channels only. While photon counting data were acquired, we discovered an electronic threshold setting issue that is currently being addressed. The maximum range performance is expected to significantly increase when the photon counting channels come on line. Figure 7 shows generally good agreement of the unedited OAWL profile with the BAO tower measurements where the SNR are sufficient (below 120m altitude). Figures 8-11 show sequential profiles that have been edited by removing constituent profiles exhibiting T0 contrast < 0.4 or atmospheric return contrast < 0.04 . Very clear (i.e. low aerosol) and westerly wind conditions prevailed during this period.

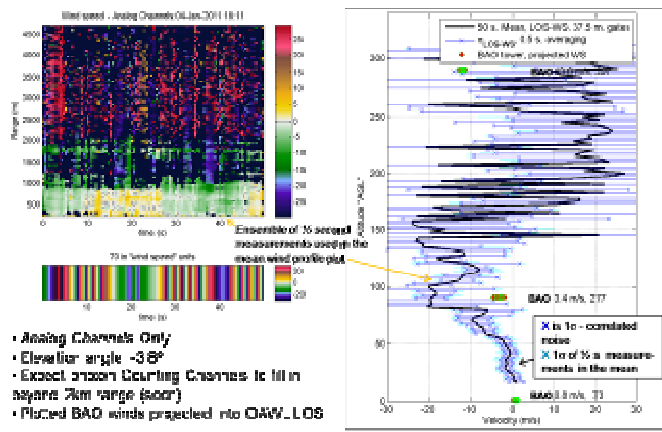


Figure 7 First (preliminary, unedited) OAWL line of sight (LOS) analog channel wind measurements plotted in m/s (color) against LOS range (m) as individual 1/2 s averaged profiles (upper left), and as a mean of the 50 s ensemble of the 1/2s profiles as a function of AGL altitude (m, right). The teal bars about the mean indicate 1σ of the 1/2s measurements, while the darker blue bars indicate 1σ of the 1/2s constituents with estimated correlated noise (e.g. due to wind turbulence) removed. Also shown in green are the 10m, 100m, and 300m BAO tower measurements with the true speed and direction indicated. The green markers have been projected into the lidar pointing direction. The width of the green markers indicates 1σ of the anemometer measurements over a 1 minute period. The lower left panel shows the corresponding T₀ OACF phase (converted to LOS velocity) demonstrating that the independence of the retrieved atmospheric wind velocities from the T₀ phase.

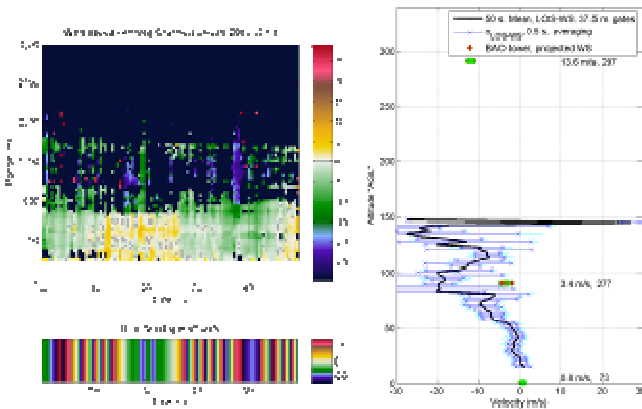


Figure 8 Same as Figure 7, but with the plotted data thresholded on a T₀ contrast >0.4 and an atmospheric return contrast >0.04.

Figure 12 plots together the mean profiles from Figures 8-11 along with the most contemporaneous BAO tower data. The rend numbers indicate the sequential order of these profiles. Note the excellent agreement below 50m altitude. Between 80m and 120m there is a jet-like structure indicated that may be real due to turbulence in the mountain valley. The sequential evolution suggests this is feasible, but the BAO tower cannot be used for verification due to its poor vertical resolution and location.

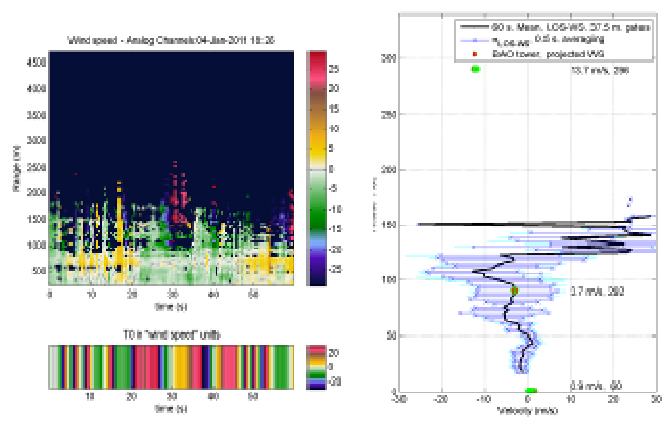


Figure 9 Same conditions as previous, but a few minutes later.

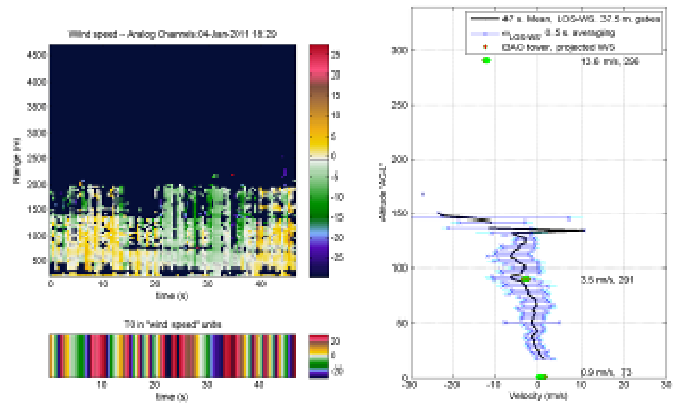


Figure 10 Same as previous, but a few minutes later.

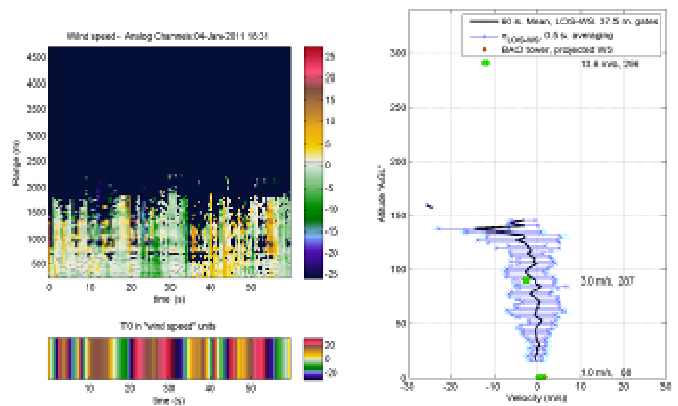


Figure 11 Same as previous, but a few minutes later.

On another day, moderate snowfall conditions were observed. These data are plotted in Figure 13. On this day, there were some issues with the alignment of the T₀ path that were subsequently discovered that affected the relationship between the T₀ and atmospheric OACF phase, the data do show that the OAWL measurements are sensitive to aerosol scattering as expected and that the statistical fluctuations of short term easurements about the mean improve with increasing backscatter (SNR).

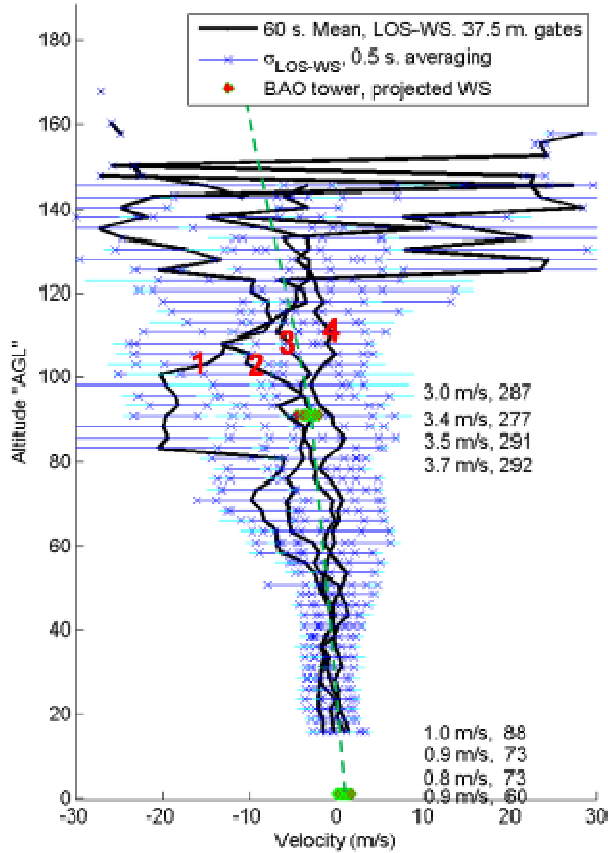


Figure 12 The 4 previous mean profiles are plotted together with the red numbers indicating the sequence order. It is not infeasible that the jet-like structure above 80m is real since it systematically varies in time while the lower profiles match closely, and maybe due to the difference in terrain between the OAWL and BAO tower venues.

5. IIP TEST PLANS

After the shake-out testing is complete the IIP program calls for two rigorous testing and validation periods. The first validations will be provided by ground testing alongside the well characterized NOAA mini-MOPA coherent detection DWL system. These tests will be conducted at the NOAA Table Mountain facility just north of Boulder, CO. The ground testing preparations are complete and currently scheduled for May 2011.

In July 2011, we plan to execute high altitude flight tests that we expect will result in raising the OAWL technology to TRL-5. An overview of the flight test plan is given in Figure 14. The plan includes flights out of Houston to and from Boulder, CO, circling several wind profilers in the NOAA network. The system does not include a scanner, so the flight path will carry the beam path (nominally 45° to vertical) about each profiler simulating a scan and allowing the vector wind profile to be derived. The flight path will cover a variety of terrain and ocean

backgrounds, likely providing observation opportunities under different cloud conditions. Higher temporal and spatial resolution profiles of the lower troposphere will also be provided by one of the NOAA coherent detection DWL systems in the Boulder area during over flights.

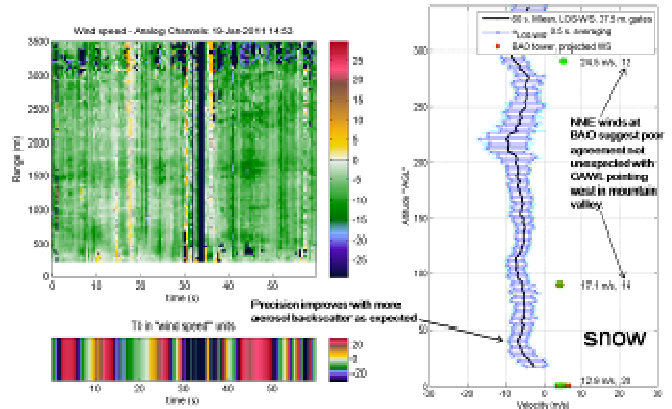
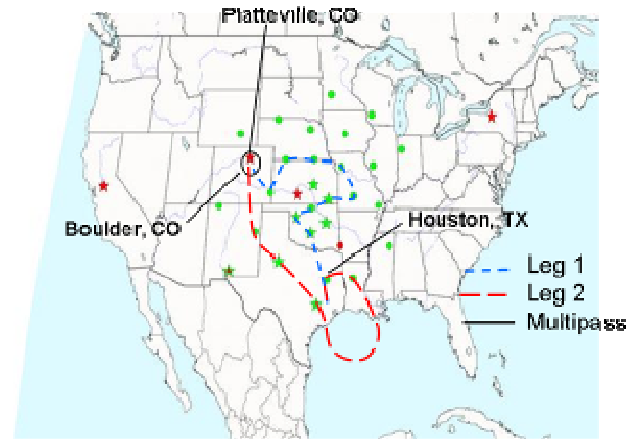


Figure 13 On another day, moderate snowfall conditions were observed demonstrating that the OAWL direct detection system is indeed primarily sensitive to aerosol backscatter and the velocity deviation between 1/2s measurements decrease significantly with backscatter. Discrepancy between the BAO measurements and OAWL may be because of the northerly winds and terrain differences or a recently noted variation in the T₀ phase relationship with relative alignment that is being addressed.



** Wind profilers in NOAA operational network

Figure 14 The airborne test plan the OAWL IIP system includes flights out of Houston to and from Boulder, CO, circling many wind profilers in the NOAA network. The flight path will cover a variety of terrain and ocean backgrounds, hopefully providing observations under different cloud conditions. Higher temporal and spatial resolution profiles will also be provided by a coherent detection DWL systems in the Boulder area.

6. NEXT STEPS

After successful ground testing, the OAWL system will be installed in the WB-57 pallet along with air circulation and thermal environmental control components. For the

WB-57 flight tests, the data system has to collect geolocation and attitude information provided by the WB-57 platform via an AIRINC interface, as well as housekeeping and health and status data from the instrument itself including a backup accelerometer to determine the OAWL attitude. For the flight tests, the system must also run in a fully autonomous mode. Significant effort will be dedicated in the next few months to developing control algorithms and testing OAWL operation over all conceivable flight conditions including brief and extended power outages. In the event of complete power failure to the pallet, insulation and thermal mass are sufficient to keep the system above survival temperature for at least 1 hour under worst case conditions while the plane descends and lands.

7. CONCLUSIONS

A complete OAWL wind lidar system has been built that is suitable for aircraft testing and incorporates in a demonstrable way many of the system design features required for a space-flight-path sensor that is scalable directly to a sensor meeting the 3D-Winds mission requirements. First preliminary wind profiles have been acquired during engineering check out in preparation for rigorous ground validations against a well characterized NOAA Doppler lidar system. These data show that we still have some work to do to achieve expected full performance, but are in general good agreement with BAO tower measurements, despite the disparate observation volumes and terrain differences. Following ground testing the system will be installed in a WB-57 flight pallet and flown at high altitude in an autonomous operating mode. Flight validations will be accomplished by comparing OAWL wind profiles to multiple NOAA wind profiler network data for a variety of aerosol and cloud conditions along the flight path, and also against a ground-based DWL operated by NOAA near Boulder, CO. A successful test program will result in availability of an alternative, single laser Integrated Direct Detection (IDD) "hybrid" architecture for the 3-D winds mission that promises to save significant cost, mass, and power, while

offering the potential to combine 3-D winds and other important environmental missions [12].

8. REFERENCES

- [1] A Community Assessment and Strategy for the Future, NRC; Earth Science and Applications from Space: National Imperatives for the Next Decade and Beyond. The National Academies Press, 2007.
- [2] Hardesty, et al, Providing global wind profiles – the missing link in today's observing system, 2005. <http://space.hsv.usra.edu/LWG/Splash%20Papers/Hardesty.pdf>
- [3] C. J. Grund, J. Howell, R. Pierce, and M. Stephens, "Optical Autocovariance Direct Detection Lidar for Simultaneous Wind, Aerosol, and Chemistry Profiling from Ground, Air, and Space Platforms", Paper 7312-37:SPIE Defense & Security Sensing Symposium; conference on Advanced Environmental, Chemical, and Biological Sensing Technologies VI, 2009
- [4] M.J. Kavaya, G.J. Koch, J. Yu, B. Trieu, F. Amzajerdian, U.N. Singh, M. Petros, "IIP Update: A Packaged Coherent Doppler Wind Lidar Transceiver "Doppler Aerosol WiNd lidar (DAWN)" <http://space.hsv.usra.edu/LWG/Jun06/Papers.jun06/Kavaya1.jun06.ppt>
- [5] Gentry, B.M., et al, Wind measurements with 355-nm molecular Doppler lidar, *Opt. Let.*, 25, 1231-1233, (2000).
- [6] Grund, et al (2007): Optical Autocovariance Wind Lidar and Performance from LEO, 14th CLRC. Available from: <http://space.hsv.usra.edu/CLRC/presentations.html>.
- [7] Schwiesow, and Mayor (1995): Coherent Optical Signal Processing for a Dop. Lidar using a Michelson Interferometer, *OSA 1995 Tech. Dig. Series*, 19, WA5-1 - WA5-4.
- [8] Bruneau, D., (2001): Mach-Zehnder interferometer as a spectral analyzer for molec. DWL, *Appl.Opt.* 40, 391-399.
- [9] Weimer, C., et al, (2007): Commissioning of the CALIPSO Payload, in publication, **SPIE 65550J-1**.
- [10] Martin Endemann ADM-Aeolus: the first spaceborne wind lidar. *SPIE Proceedings Vol. 6409*, (2006).
- [11] Courtesy of Bruce Gentry, NASA/GSFC.
- [12] Grund, et al Supporting NOAA and NASA High-Performance space-based DWL objectives with a min. cost, mass, power, and risk approach employing OAWL. Feb 2008 Working group on Space-Based Lidar Winds, 2008: <http://space.hsv.usra.edu/LWG/Index.html>.